Experimental investigation and statistical optimisation of the selective laser melting process of a maraging steel

Experimental investigation and statistical optimisation of the selective laser melting process of a maraging steel

G. Casalino, S.L. Campanelli, N. Contuzzi, and A.D. Ludovico

Department of Mechanics, Mathematics and Management, Politecnico of Bari, Bari, Italy; g.casalino@poliba.it

ABSTRACT

Selective Laser Melting (SLM) is an Additive Manufacturing process that built parts from powder using a-layer-by-layer deposition technique. A careful control of the parameters which influence the melting and the amount of energy density involved in the process is necessary to get valuable parts. The objective of this paper is to perform an experimental optimization of the process parameters supported by statistical methods. The microstructure, mechanical and surface properties of 18 Ni 300 SLM steel parts were analyzed. The analysis of variance was used to study the effects of laser power and scan speed on relative density of built parts, hardness, mechanical strength and surface roughness. The correlation between the relative density and the other output factors was also investigated.

After the statistical analysis the optimization of the process parameters was done through the contour plot of the relative density.

KEYWORDS: Selective Laser Melting, statistical analysis, microstructure, mechanical properties, surface roughness, optimization.

1. INTRODUCTION

Selective laser melting (SLM) is probably the most rapidly growing technique in rapid prototyping (RP) and rapid manufacturing technologies. It uses 3D computer aided design data as a digital information source and energy in the form of a high powered laser beam to create three-dimensional metal parts by fusing together a fine metallic powder [1]. SLM represents an evolution of the Selective Laser Sintering (SLS) process that was developed and patented by Carl Deckard and Joe Beaman at the University of Texas at Austin in the mid-1980s for producing plastic prototypes. SLM started at the Fraunhofer Institute for Laser Technology ILT in Aachen, Germany, in 1995 with a German research project, resulting in the so called basic ILT SLM patent DE 19649865 [2, 3]. The SLM process is the same as SLS except for the much

https://doi.org/10.1016/j.optlastec.2014.07.021

higher laser energy density required. The amount of energy density causes the powder to fully melt in SLM and to superficially melt in SLS. In SLM, nearly full density parts can be produced without the need of post-processing steps. In recent years, the process has been optimized in order to build parts not only for prototyping purposes but also for productions [4, 5].

Nowadays the main objective in this field is to produce parts with mechanical properties comparable with those of components produced with traditional processes. These properties depend on composition and size of the powder as well as the process parameters and manufacturing strategy [6-7].

Several materials have been successfully investigated with SLM process such as hard tool steels [8, 9], stainless steels [10, 11], composites of Al–Si–Mg/SiC, stainless steel/hydroxyapatite, 663 copper alloy, Fe–Ni–Cr and TiC/Ti5Si3 [12–16], Ni based alloys [17-19] and recently also Ti [20-22] and Mg alloys [23].

The goal of this study was to investigate the Nd:YAG SLM process of 18 Ni Marage 300. The quality of laser sintered part was evaluated in terms of microstructure, density, mechanical properties and surface roughness. Through the analysis of variance (ANOVA) the main effect and the two factor interactions, i.e. laser power and scan speed, on the investigated output factor were studied. The correlation between the relative density (ρ_r%) of built parts and hardness (HRC), ultimate tensile strength (UTS), elongation to break and surface roughness (SR) was studied. The optimal process parameters were selected.

2. EXPERIMENTAL PROCEDURE

For this investigation all the experimental tests were carried out on a laser machine equipped with a Nd:YAG laser source characterized by a 1.064 μm wavelength, 200 μm spot diameter of and a maximum output power of 100 W. The laser light was moved over the powder surface by means of scanning mirrors in order to draw selectively every layer of the powder.

The powder deposition system consisted of a working platform and a coater that deposited powder layers in one direction (Figure 1). The powder chamber was filled with nitrogen to avoid oxidation of the parts and to reduce the initial oxygen level at 0.8%.

https://doi.org/10.1016/j.optlastec.2014.07.021

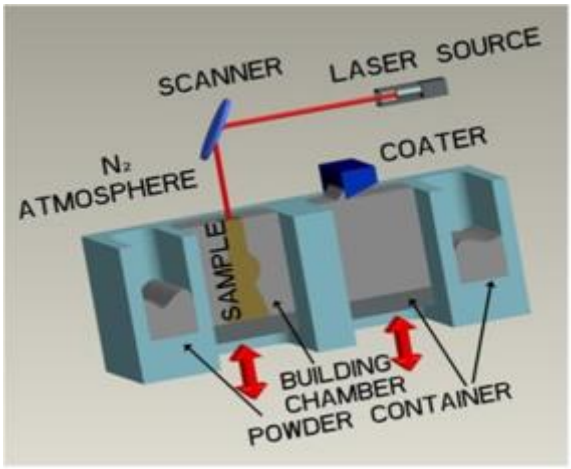

Fig. 1. A scheme of the SLM Process.

The investigated 18 Ni Marage 300 steel is included in the category of maraging steels that comprise a special class of high-strength steels that differ from conventional steels in that they are hardened by a metallurgical reaction that does not involve carbon. These steels are strengthened by the precipitation of intermetallic compounds at temperature of about 480°C. The term maraging is derived from martensite age hardening ad denotes the age hardening of a low-carbon, iron–nickel lath martensite matrix. Maraging steels are also age–hardenable in the 400-650°C temperature range. The aging below 450°C produces ordered and coherent phases in a martensitic matrix [24, 25].

18 Ni Marage 300 steel has excellent mechanical properties, high values of yield strength and tensile strength, high toughness, ductility and toughness, high fatigue limit, high compressive strength, hardness and wear resistance.

The powder was produced with particles of different size ranging since few micron to the maximum size of 40μm (figure 2). Previous studies showed that a spherical particle is necessary to obtain a good distribution of the powder on the building platform and a different size allows getting better adhesion during melting.

The chemical composition of the powder was studied by Energy Dispersive X-ray (EDX) analysis and it is reported in Table 1.

https://doi.org/10.1016/j.optlastec.2014.07.021

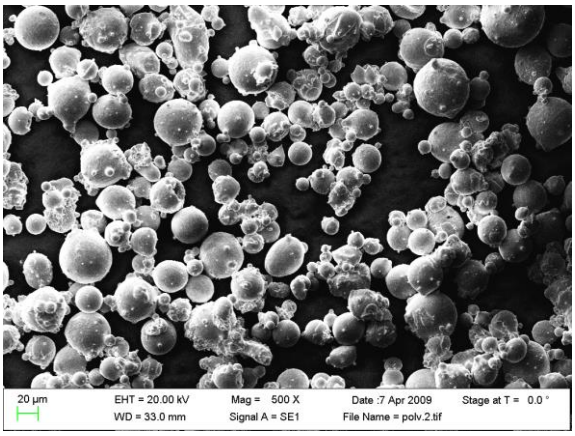

a)
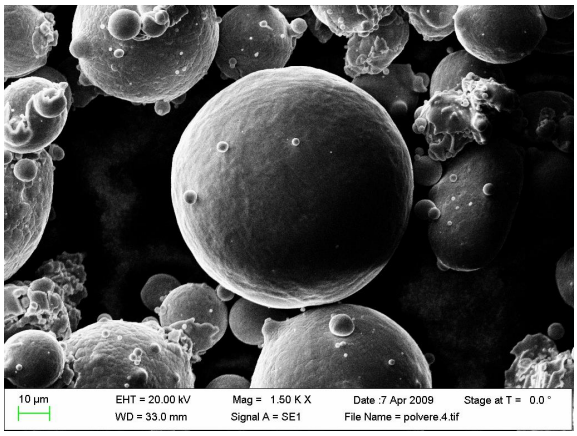

b)

Fig. 2. Scanning electron micrographs of the as-received .

Table 1
Chemical composition of the employed powder determined by EDX analysis.

Powder Material	Ni	Mo	Co	Ti	C	Fe
18 Ni Marage 300	18.8	4.2	10.2	0.88	0.02	Balance

Many of the input parameters of SLM can be controlled and varied in order to get parts with optimized quality. Some of these parameters are: layer thickness, scan speed, scan spacing, scanning strategy, powder characteristics (size, distribution, shape, etc.) and laser parameters (power, spot size, etc.). Particularly, the success of a product manufactured with SLM process requires a thorough control of the parameters which influence the melting and the amount of energy density involved in the process.

A full factorial plan was designed for the simultaneous study of the effects of the involved parameters on the success of the SLM in terms of relative density, surface roughness, hardness, UTS and elongation to break. The factorial design was characterized by two factors (laser power and scanning speed), with 3 levels for laser power and 3 levels for scan speed for a total of 9 combinations of the parameters.

The other process parameters were kept constant. Hatch spacing, that is the distance between two adjacent scan vectors was set to 140 µm allowing a certain degree of overlapping necessary to guarantee a high value of density; layer thickness, that is the depth of a layer, determined by the stepping of the working platform, was set to 30 µm to improve accuracy of parts and to get better adhesion between layers.

The single track energy density (E_d) can be calculated by the relation between laser power (P), scan speed (v) and spot diameter (d) (Equation 1) [8]:

https://doi.org/10.1016/j.optlastec.2014.07.021

$$E_d = \frac{P}{v \cdot d}\left[\frac{J}{mm^2}\right] \qquad (1)$$

where:

- P is the laser power used to scan a part;
- v is the scan speed or the velocity of laser beam scan.

Table 2
Experimental plan.

	Laser Power [W]	**Scan Speed [mm/s]**	**Energy Density [J/mm^2]**
1	57	180	1.58
2	86	200	2.15
3	86	180	2.39
4	100	200	2.50
5	100	220	2.27
6	57	220	1.29
7	100	180	2.78
8	57	200	1.42
9	86	220	1.95

The adopted experimental plane and values of the energy density for each combination of the parameters are showed in table 2.

Small square samples of 15mm x 15mm x 10mm were built to measure density and hardness, and to study microstructure (Fig. 3a).

Early studies on SLM showed that appropriate scanning patterns produce an appreciable reduction in thermal deformations. Thus in order to produce parts with low residual stresses, the scanning strategy was optimized by dividing the part area in small square sectors of 5×5 mm^2. Furthermore, a random scanning sequence was chosen to melt each sector.

https://doi.org/10.1016/j.optlastec.2014.07.021

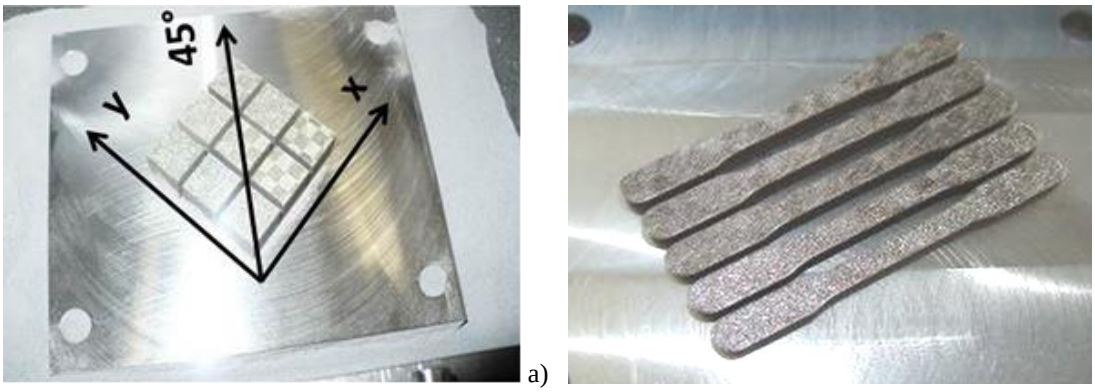

a)

b)

Fig. 3. a) square SLM built samples of 15mm x 15mm x 10mm used to measure density, hardness, surface roughness and to study microstructure; b) tensile test specimens according to ASTM E 8M–04 [26].

Density tests were performed in order to evaluate the presence of porosities variation of the Density was measured with the 'Archimedes-method' by weighting the samples in air and subsequently in demineralized water.

Roughness tests were performed on all samples along the x, the y and the 45° directions, as illustrated in figure 3 in order to determine its average value on the xy plane for all combinations of process parameters. The R_a index was measured for roughness using the Taylor-Hobson Surtronic 25 instrument and values of R_a were collected.

Rockwell C test was used for hardness.

Mechanical properties were determined performing tensile tests (according to the ASTM E 8M – 04 standard) using an Instron 4467 machine equipped with an extensometer (with a 12.5mm gauge length and maximum elongation of 5 mm). The size of the parts was chosen according to the dimension suggested by the STM standard (Fig. 3b) [26]. Values of Ultimate Tensile Strength (UTS) and of Elongation to break (ε_b%) were collected to estimate the mechanical behavior of the material.

3. PHYSICAL CHARACTERIZATION

3.1 Relative density

The effect of Energy Density on Relative Density (Figure 4) was plotted and analyzed. Values of E_d ranges from 1.29 to 2.78 J/mm^2. It is evident that density of parts increase with E_d, reaching average values higher than 99%. The true density of the material is 8.01 g/cm^3; this clearly indicates that ρ% of built parts changes between 90.9 and 99.9%, obtaining nearly the full density. The average maximum value can be obtained for E_d = 2.78 J/mm^2.

https://doi.org/10.1016/j.optlastec.2014.07.021

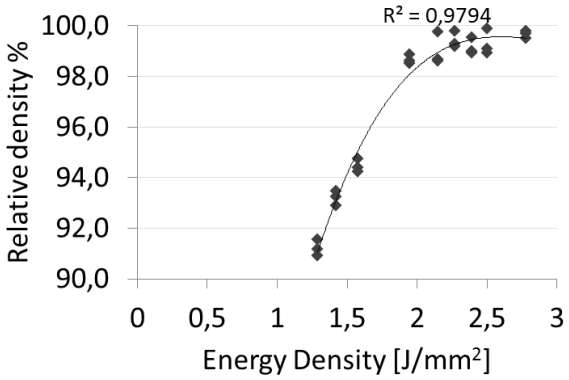

Fig. 4. Density as function of the Energy Density.

Samples for metallographic examinations were cut, ground and polished according to standard procedures. The cross-section macrostructures of 18 Ni Marage 300 steel parts processed using the different SLM parameters, according to Table 2, are provided in Figure 5. Micrographs were detected using an optical microscope with a 100 X magnification.

Samples 2, 3, 4, 5, 7 and 9, having a relative density more or less 99%, show small closed pores with almost regular shape. Sample 1, 6, and 8, having average value of 94.5% and 93% of ρ% between 91% and 94.5%, show larger pores with irregular shape.

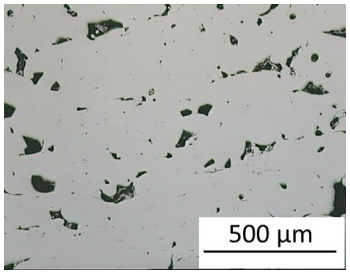	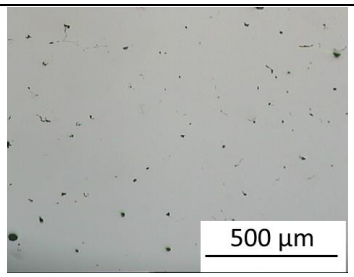	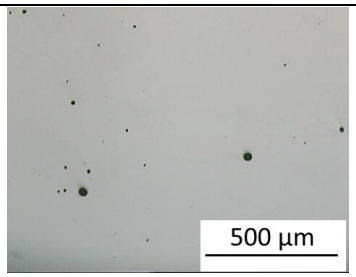
sample 1 ρ% = 94.5%	sample 2 ρ% > 99%	sample 3 ρ% > 99%
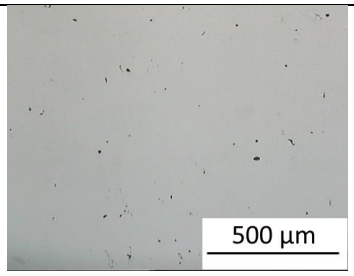	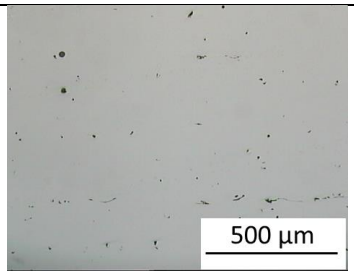	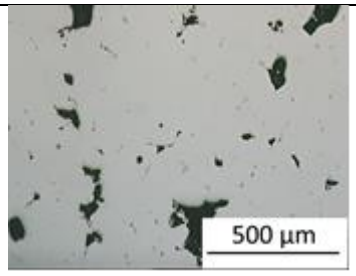
sample 4 ρ% > 99%	sample 5 ρ% > 99%	sample 6 ρ% = 91%

https://doi.org/10.1016/j.optlastec.2014.07.021

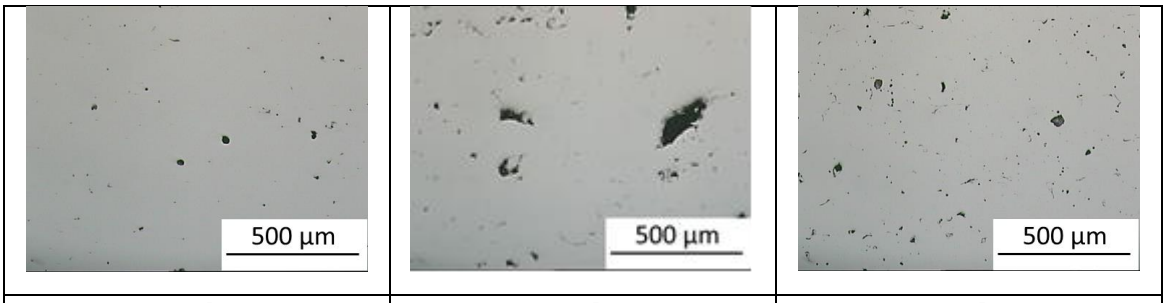

sample 7	sample 8	sample 9
ρ% > 99%	ρ% = 93%	ρ% = 98.6%

Fig. 5. Cross-section macrostructures of 18 Ni Marage 300 steel parts processed using the different SLM parameters according to Table 2 (magnification 100x).

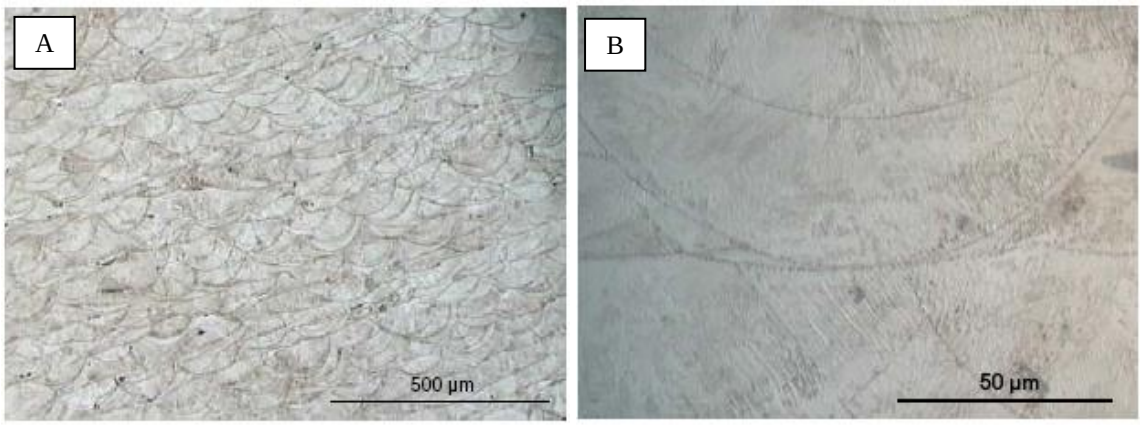

Fig. 6. 100x magnification of sample 5 (A);1000x magnification of sample 7 (B).

3.2 Microstructure

After polishing the samples were etched with 2%Nital in order to reveal microstructure. Figs 6a) and 6b) show, respectively, micrographs at magnifications 100X and 400X obtained with an optical microscope. It is evident that the metal powder is completely fused and constituted from molten/resolidified zones with curved edges (approximately parabolic). The laser tracks overlap in order to reduce porosity. This means that each part is welded onto the layers that surround it. Figure 7 show scanning electron microscopy (SEM) micrographs of sample 5 at different magnifications. A very fine solidification structure can be detected. Different kind of grains can be observed: equi-axed grains smaller than 1 µm and columnar grains; this is probably due to the different thermal gradients because of the overlapping of laser tracks. Intercellular spacing is less than 1µm and this contributes to very good strength and hardness. Similar results were found by other researchers working on direct metal laser sintering of maraging steel 300 processed on an EOS machine [27] and on Concept Laser M3 Linear SLM machine [9].

https://doi.org/10.1016/j.optlastec.2014.07.021

Sample 5 has a relative density higher than 99%, so the presence of pores (black spots) is very limited and appears to be closed and almost circular with a dimension smaller than 30 μm.

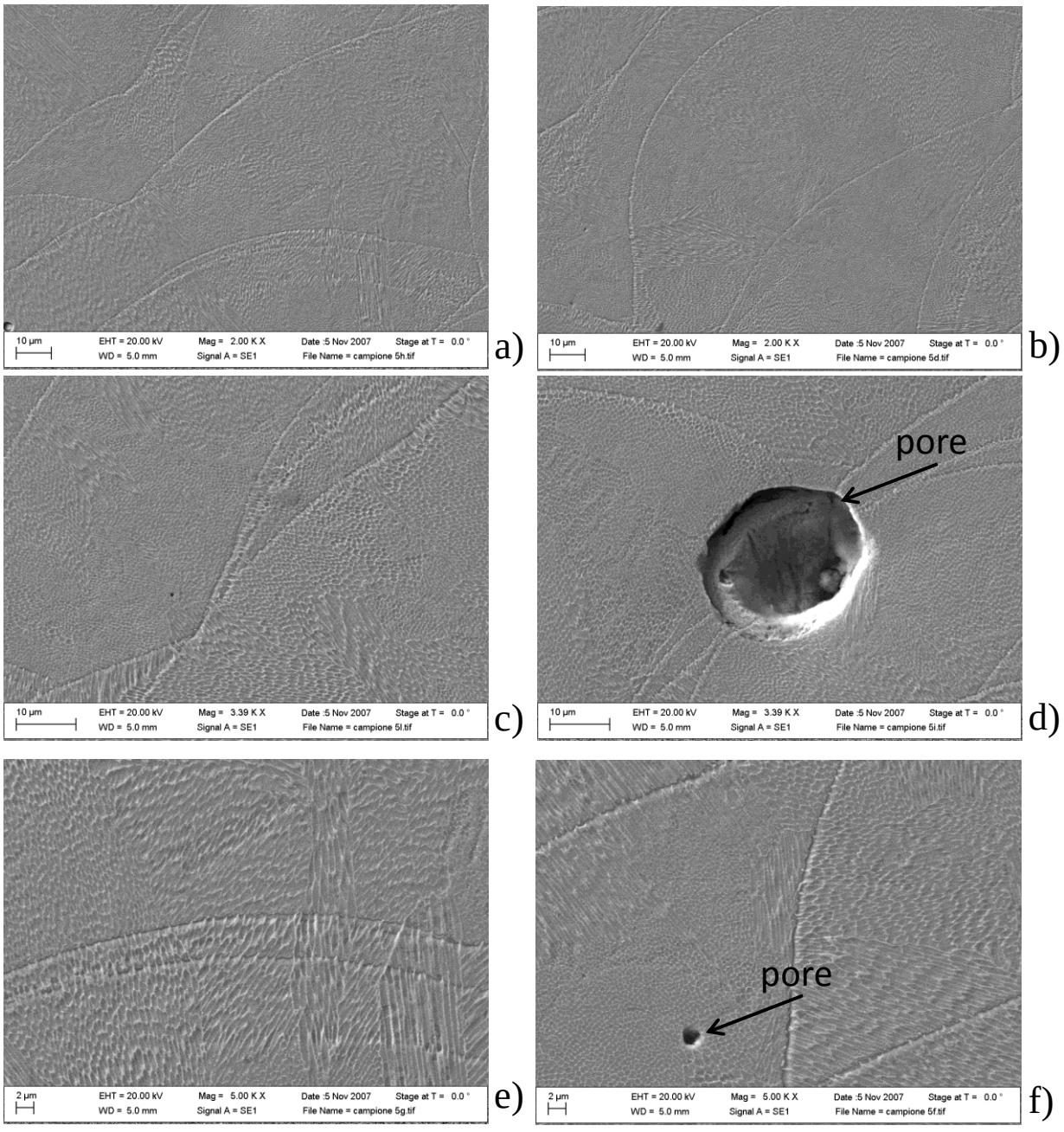

Fig. 7. Scanning electron microscope (SEM) micrographs of sample 5 at different magnifications: a) and b) 2000x, c) and d) 3390x, e) and f) 5000x. (mettere l'ingrandimento sulle figure e non nellla didascalia

3.3 Tensile test

Tensile Test was performed on a standard Ingstrom tensile tester at room temperature. In Figure 8 are shown the representative trends of stress-strain curves for three different relative densities.

https://doi.org/10.1016/j.optlastec.2014.07.021

As it was expected the tensile test results show that the ultimate and yield tensile strength, as well as elongation depend on the relative density. The behavior of the specimens with the low relative densities (94.5% and 91%) was weak while the specimen with 99% density had very better ultimate strength and elongation.

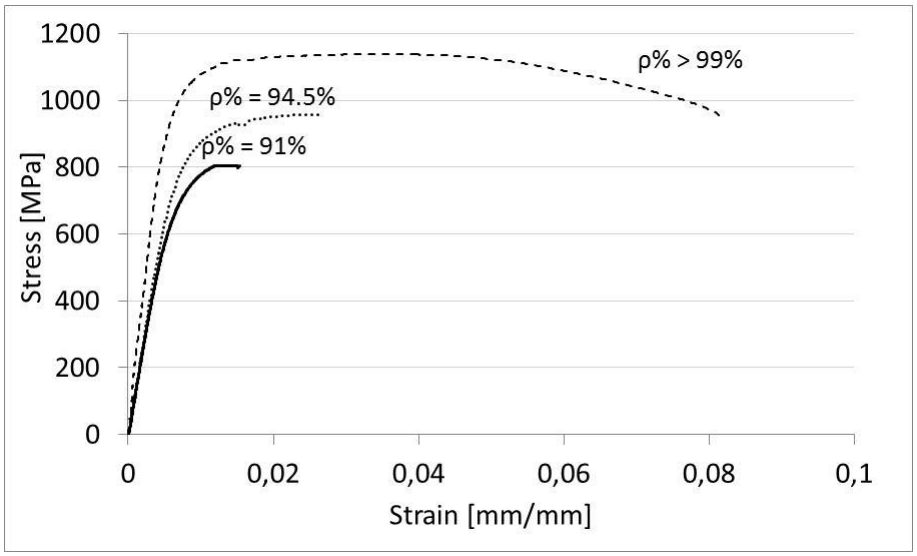

Fig. 8. Stress-strain curves for different densities.

Fracture surfaces after tensile tests are given in figure 9. After Manfredi et al. [28] it may be assumed that the ductile fracture is the result of growth and coalescence of micro-voids. The fragile fracture was due to the macro-voids that formed during the laser sintering process.

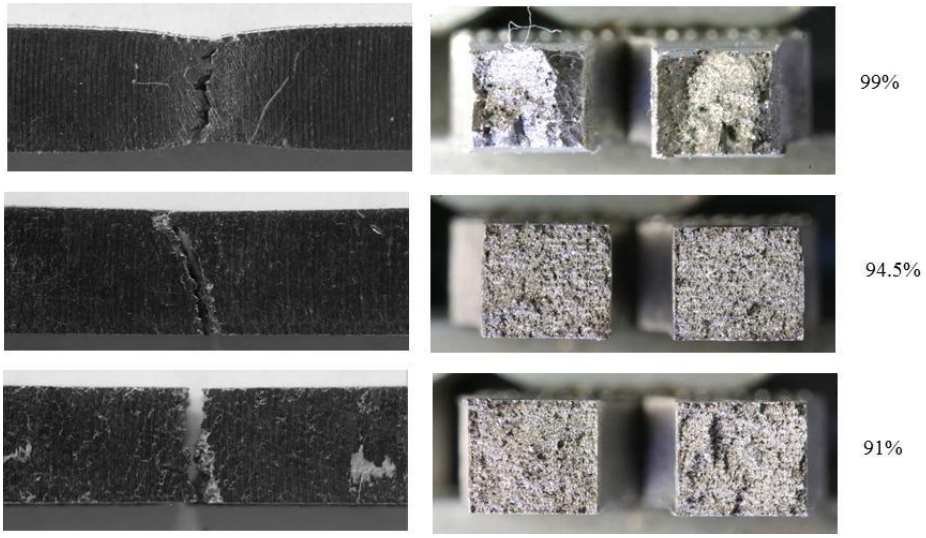

Fig. 9. Fractured samples (left) and fracture surfaces (right).

https://doi.org/10.1016/j.optlastec.2014.07.021

4. STATISTICAL ANALYSIS AND OTIMIZATION

In order to investigate the influence of the considered factors on the quality of the parts, the Analysis of Variance (ANOVA) was performed. The investigated factors were the relative density, the ultimate tensile strength, the hardness and surface roughness.

The General Linear Model was used to perform ANOVA. The data set is balanced because it contains the same number of observations for each combination of factor levels. Factors for this model are discrete variables, therefore the ANOVA examines whether the variance of the factor is zero. The p-value tells whether the effect for that term is significant. If the effect of a discrete factor is significant, then the variance of the factor is not zero.

The level of significance represents the smaller the value for which the process parameters and their interactions are statistically significant on the value of the output. If a calculated p-value is greater than the level of significance the effect of the parameter is judged not to be significant.

The results of ANOVA are summarized in Tables 3, 4, 5, 6 and 7. The p-values are very small for all the main effects and they are very little for most of the first order interactions. When a 0.05 level of significance is chosen, the process parameters and their interactions are statistically significant for $\rho_r\%$, hardness and *UTS* while only the main effects are statistically significant for $\varepsilon_b\%$ and *SR*.

Table 3

Analysis of variance for relative density $\rho_r\%$.

Factors	Seq SS	Adj SS	Adj MS	F	p-value
P	234.407	234.407	117.203	857.59	0.000
v	7.762	7.762	3.881	28.40	0.000
P v	8.718	8.718	2.179	15.95	0.000

Table 4

Analysis of variance for hardness HRC.

Factors	Seq SS	Adj SS	Adj MS	F	p-value
P	1284.20	1284.20	642.10	152.57	0.000
v	32.05	32.05	16.02	3.81	0.042
P v	73.57	73.57	18.39	4.37	0.012

https://doi.org/10.1016/j.optlastec.2014.07.021

Table 5

Analysis of variance for *UTS*.

Factors	Seq SS	Adj SS	Adj MS	F	p-value
P	314751	314751	157375	59.79	0.000
v	22925	22925	11462	4.36	0.029
P v	38077	38077	9519	3.62	0.025

Table 6

Analysis of variance for ε_b%.

Factors	Seq SS	Adj SS	Adj MS	F	p-value
P	108.92	108.92	54.459	65.21	0.000
v	6.880	6.880	3.440	4.12	0.034
P v	0.960	0.960	0.240	0.29	0.882

Table 7

Analysis of variance for *SR*.

Factors	Seq SS	Adj SS	Adj MS	F	p-value
P	116.15	116.15	58.75	69.54	0.000
v	19.681	19.681	9.840	11.78	0.001
P v	3.929	3.929	0.982	1.18	0.355

After the analysis of the variance, a correlation analysis was performed to evaluate the degree of the relation between the relative density and the mechanical, i.e. hardness HRC, UTS and ε_b%, and surface properties of the built samples.

As showed in Figure 8, the mechanical properties correlate positively with the relative density. Otherwise, the surface roughness correlates negatively with the relative density.

The coefficients of determination for the linear models are equal or greater than 0.8, which indicates how well data points fit a line or curve.

The higher mechanical properties and the lower surface roughness were obtained for the higher levels of the relative density. Therefore, the optimization of the process parameters, which would be otherwise complex, can be simplified to the optimization of the relative density.

https://doi.org/10.1016/j.optlastec.2014.07.021

The latter problem is easily worked out by observing the contour plot in figure 9. This graph represents a map by which correct combinations of laser power and scan speeds can be selected.

Almost free porosity samples can be obtained with the laser power above 90 W and all the scan speeds in the investigated range of velocity (180-220 mm/s). It is also predictable that for velocity faster than 220 mm/s the power laser should be stronger than 90 W to obtain a 99% relative density part.

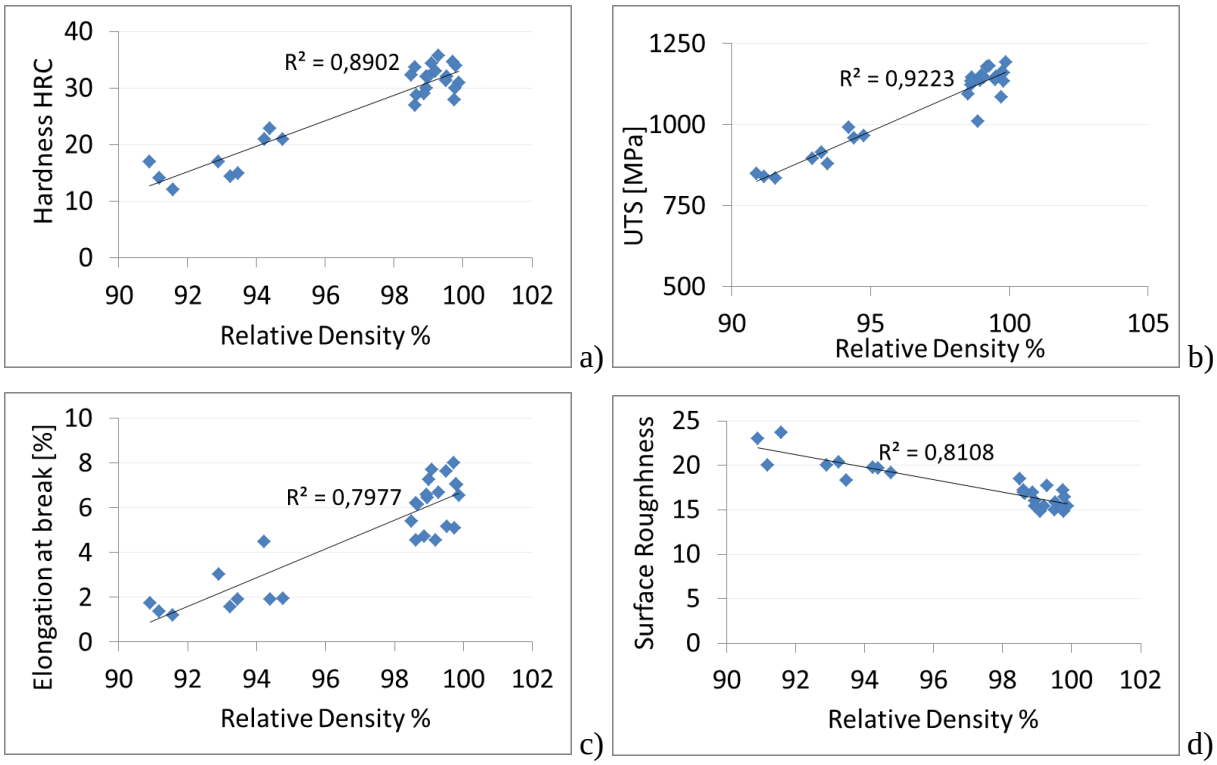

Fig. 10. Correlation diagrams between the mechanical properties, the surface roughness and the relative density.

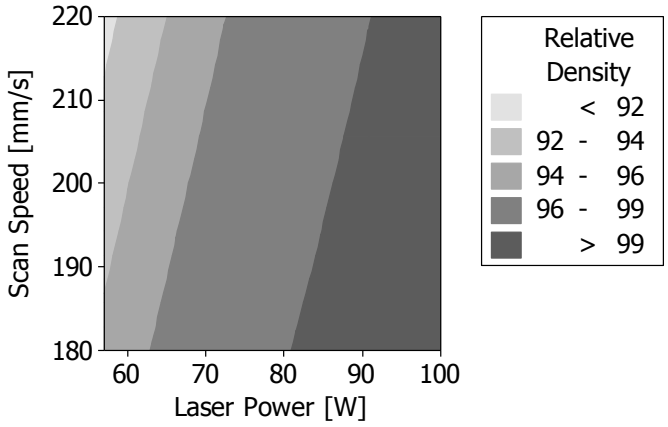

Fig. 11. Contour plot for the relative density [%] and the process parameters.

https://doi.org/10.1016/j.optlastec.2014.07.021

Mechanical properties of SLM parts obtained with $\rho_r\% > 99.7\%$ are coherent with those reported in ASM Handbook [25] for typical range of mechanical properties developed in unaged 18 Ni maraging steels after solution annealing (Table 8).

Table 8

Mechanical properties for 18 Ni marage 300 wrought and SLM steel.

	UTS	$\varepsilon_b\%$	HRC
Wrought 18 Ni Marage 300	1000-1170	6-17	30-37
SLM 18 Ni Marage 300 ($\rho_r\% > 99.7\%$)	1085-1192	5-8	30-35

5. CONCLUSION

This paper describes an experimental analysis performed on the 18 Ni marage 300 steel built by the Selective Laser Melting technology.

Results for relative density showed that parts with $\rho_r\% > 99$ could be built; furthermore it was found that $\rho_r\%$ increases with energy density. The parts, that had a relative density higher than 99%, were characterized by very low porosity with closed and regular shape pores, with dimension smaller than 30 μm. Their tensile properties and fracture behavior were improved by a high level of the relative density. The Analysis of Variance indicated that scan speed and laser power and their interactions are statistically significant for $\rho_r\%$, hardness and *UTS* otherwise only the main effects are statistically significant for $\varepsilon_b\%$ and *SR*, choosing a level of confidence of 95%.

A positive correlation was demonstrated between the mechanical and the relative density. Therefore, the optimization of the process parameters was performed by analyzing the contour plot of the relative density. The area in which the relative density was higher than 99% was defined from a laser power bigger than 90 W and a velocity smaller than 220 mm/s.

REFERENCES

[1] J.P. Kruth, P. Mercelis, J. Van Vaerenbergh, L. Froyen, M. Rombouts, Selective laser melting of iron-based powder, Journal of Materials Processing Technology, Vol. 149, (2004), 616–622

https://doi.org/10.1016/j.optlastec.2014.07.021

[2] H. Schleifenbaum, A. Diatlov, C. Hinke, J. Bültmannn, H. Voswinckel: Direct photonic production: towards high speed additive manufacturing of individual goods. Production Engineering – Research and Development 5 (2011) 359 – 371.
[3] H. Schleifenbaum, W. Meiners, K. Wissenbach & C. Hinke: Individualized production by means of high power selective laser melting, Cirp Journal of Manufacturing Science Technology 2 (2010) 161–169.
[4] L. Lu, J.Y.H. Fuh,. & Y.S. Wong, Laser-Induced materials and processes for rapid prototyping, Kluwer Academic publishers, ISBN 0-7923-7400-2, Boston, 2001.
[5] M. Badrossamay, T.H.C. Childs, Further studies in selective laser melting of stainless and tool steel powders, *International Journal of Machine Tools & Manufacture*, Vol. 47 (2007) 779–784.
[6] Casavola, C.; Campanelli, S.L.; Pappalettere, C. Preliminary investigation on the residual strain distribution due to the Selective Laser Melting Process. Journal of Strain Analysis 2009, 44, 93-104.
[7] S.L. Campanelli, N. Contuzzi, A. Angelastro & A.D. Ludovico, Capabilities and performances of the Selective Laser Melting process, New Trends in Technologies: Devices, Computer, Communication and Industrial Systems, ISBN 978-953-307-212-8, Sciyo, 2010.
[8] Campanelli, S.L.; Contuzzi, N.; Ludovico, A.D. Manufacturing of 18 Ni Marage 300 steel samples by selective laser melting. Advanced Materials Research 2010, 83–86, 850–857.
[9] K.Kempen, E.Yasa, L.Thijs, J.-P. Kruth, J.Van Humbeeck, Microstructure and mechanical properties of Selective Laser Melted 18Ni-300 steel.
[10] T.H.C. Childs, C. Hauser, M. Badrossamay Selective laser sintering (melting) of stainless and tool steel powders: experiments and modelling Proceedings of the Institution. of Mechanical Engineers, Part B: Journal of Engineering Manufacture, 219B (2005), pp. 339–358
[11] I. Yadroitsev, Ph. Bertrand, I. Smurov, Parametric analysis of the selective laser melting process, Applied Surface Science, Volume 253, Issue 19, 31 July 2007, Pages 8064–8069.
[12] Brandl E, Heckenberger U, Holzinger V, Buchbinder D. Additive manufactured AlSi10Mg samples using selective laser melting (SLM): microstructure, high cycle fatigue, and fracture behavior. Mater Des 2012;34:159–69.
[13] Hao L, Dadbakhsh S, Seaman O, Felstead M. Selective laser melting of a stainless steel and hydroxyapatite composite for load-bearing implant development. J Mater Process Technol 2009;209:5793–801.
[14] Zhang Y, Xi M, Gao S, Shi L. Characterization of laser direct deposited metallic parts. J Mater Process Technol 2003;142:582–5.
[15] Joo BD, Jang JH, Lee JH, Son YM, Moon YH. Selective laser melting of Fe–Ni–Cr layer on AISI H13 tool steel. Trans Nonferrous Met Soc China 2009;19:921–4.
[16] Gu DD, Hagedorn YC, Meiners W, Wissenbach K, Poprawe R. Selective laser melting of in-situ TiC/Ti5Si3 composites with novel reinforcement architecture and elevated performance. Surf Coat Technol 2011;205:3285–92.
[17] F. K. Osakada, M. Shiomi, K. Uematsu, M. Matsumoto, The manufacturing of hard tools from metallic powders by selective laser melting, Journal of Materials Processing Technology Volume 111, Issues 1–3, 25 April 2001, Pages 210–213.
[18] Kamran Aamir, Poonjolai Erasenthiran, Neil Hopkinson, High density selective laser melting of Waspaloy®, Journal of Materials Processing Technology, Volume 195, Issues 1–3, 1 January 2008, Pages 77–87.
[19] T. Vilaro, C. Colin, J.D. Bartout, L. Nazé, M. Sennour, Microstructural and mechanical approaches of the selective laser melting process applied to a nickel-base superalloy, Materials Science and Engineering: A, Volume 534, 1 February 2012, Pages 446-451

https://doi.org/10.1016/j.optlastec.2014.07.021

[20] B. Vandenbroucke, J.P. Kruth, Selective laser melting of biocompatible metals for rapid manufacturing of medical parts, Rapid Prototyping Journal, Vol. 13 Issue 4, pp.196 – 203, 2007.
[21] Lore Thijs, Frederik Verhaeghe, Tom Craeghs, Jan Van Humbeeck, Jean-Pierre Kruth, A study of the microstructural evolution during selective laser melting of Ti–6Al–4V, Acta Materialia,Vol. 58, Issue 9, May 2010, Pages 3303–3312.
[22] Jianfeng Sun, Yongqiang Yang, Di Wang, Parametric optimization of selective laser melting for forming Ti6Al4V samples by Taguchi method, Optics & Laser Technology, Volume 49, July 2013, Pages 118-124
[23] C.C. Ng, M.M. Savalani, M.L. Lau, H.C. Man, Microstructure and mechanical properties of selective laser melted magnesium, Applied Surface Science, Volume 257, Issue 17, 15 June 2011, Pages 7447–7454.
[24] J. M. Pardal, S. S. M. Tavares , M. P. Cindra Fonseca, M. R. da Silva, J. M. Neto, H. F. G. Abreu, Influence of temperature and aging time on hardness and magnetic properties of the maraging steel grade 300, J Mater Sci, Vol. 42 (2007), 2276–2281.
[25] ASM Handbook, Volume 1 Properties and Selection: Irons, steels and high performance alloys, 1990, ASM International, The Materials Information Company, United States of America, ISBN 0-87170-377-7 (v.1), pp.1303-1408.
[26] ASTM E 8M, Standard test methods for tension testing of metallic Materials, vol. 03.01, Metals – mechanical testing; elevated and low-temperature tests; metallography, 2004, Vol. 4, (ASTM International, West Conshohocker, Pennsylvania).
[27] Stanford, M., Kibble, K., Lindop, M., Mynors, D. and Durnall, C., 2008, An investigation into fully melting a maraging steel using direct metal laser sintering (DMLS), Steel Research Inst. 79, Special Edition Metal Forming Conference, Vol. 2, pp. 847-852.
[28] Manfredi, D., Calignano F., Krishnan, M. Canali R., Ambrosio, E. P., Atzeni, E. From Powders to Dense Metal Parts: Characterization of a Commercial AlSiMg Alloy Processed through Direct Metal Laser Sintering. Materials 2013, 6, 856-869; doi:10.3390/ma6030856.

https://doi.org/10.1016/j.optlastec.2014.07.021